Globally limited but severe shallow-shelf euxinia during the end-Triassic extinction

Andrew D. Bond [1], Alexander J. Dickson [1], Micha Ruhl [2], Remco Bos [3] & Bas van de Schootbrugge [3]

One of the most severe extinctions of complex marine life in Earth's history occurred at the end of the Triassic period (~201.4 million years ago). The marine extinction was initiated by large igneous province volcanism and has tentatively been linked to the spread of anoxic conditions. However, the global-scale pattern of anoxic conditions across the end-Triassic event is not well constrained. Here we use the sedimentary enrichment and isotopic composition of the redox-sensitive element molybdenum to reconstruct global–local marine redox conditions through the extinction interval. Peak δ^{98}Mo values indicate that the global distribution of sulfidic marine conditions was similar to the modern ocean during the extinction interval. Meanwhile, Tethyan shelf sediments record pulsed, positive δ^{98}Mo excursions indicative of locally oxygen-poor, sulfidic conditions. We suggest that pulses of severe marine de-oxygenation were restricted largely to marginal marine environments during the latest Triassic and played a substantial role in shallow-marine extinction phases at that time. Importantly, these results show that global marine biodiversity, and possibly ecosystem stability, were vulnerable to geographically localized anoxic conditions. Expanding present-day marine anoxia in response to anthropogenic marine nutrient supply and climate forcing may therefore have substantial consequences for global biodiversity and wider ecosystem stability.

The Triassic/Jurassic boundary interval (TJB, ~201 million years ago) is marked by one of the largest extinctions of complex marine life in Earth's history: the end-Triassic mass extinction event (ETME)[1]. The ETME has been closely associated with supraregional volcanism from the Central Atlantic Magmatic Province, which has been linked to atmospheric carbon injection as evidenced through Triassic–Jurassic negative carbon isotope excursions[2]. Central Atlantic Magmatic Province activity is also thought to have caused Triassic–Jurassic marine acidification and marine de-oxygenation[2,3]. Studies of Triassic–Jurassic marine biomarkers and δ^{34}S (where the delta notation (δ) is defined as the difference in isotopic ratio between a sample and

a reference standard) indicate that locally sulfidic conditions were prominent within marginal marine surface waters of the Tethys and Panthalassa oceans around the TJB[3–8]. Oxygen-poor conditions have been further identified from blooms of prasinophycean algae[3,9], a negative excursion in carbonate uranium isotopes[10,11], widespread Early Jurassic black-shale deposition[9,12], elemental redox proxies[3,13] and iron speciation data[14]. Therefore, recent studies suggest that marine redox change may have played an important role in end-Triassic marine extinction phases. However, most existing Late Triassic redox studies are at a local, basinal or sub-regional scale and do not provide information about the global-scale distribution of marine redox conditions.

[1]Department of Earth Sciences, Royal Holloway University of London, Egham, Surrey, UK. [2]Department of Geology, School of Natural Sciences, Trinity College Dublin, The University of Dublin, Dublin, Ireland. [3]Department of Earth Sciences, Marine Palynology and Paleoceanography, Utrecht University, Utrecht, the Netherlands. ✉e-mail: Andrew.Bond.2019@live.rhul.ac.uk; Alex.Dickson@rhul.ac.uk
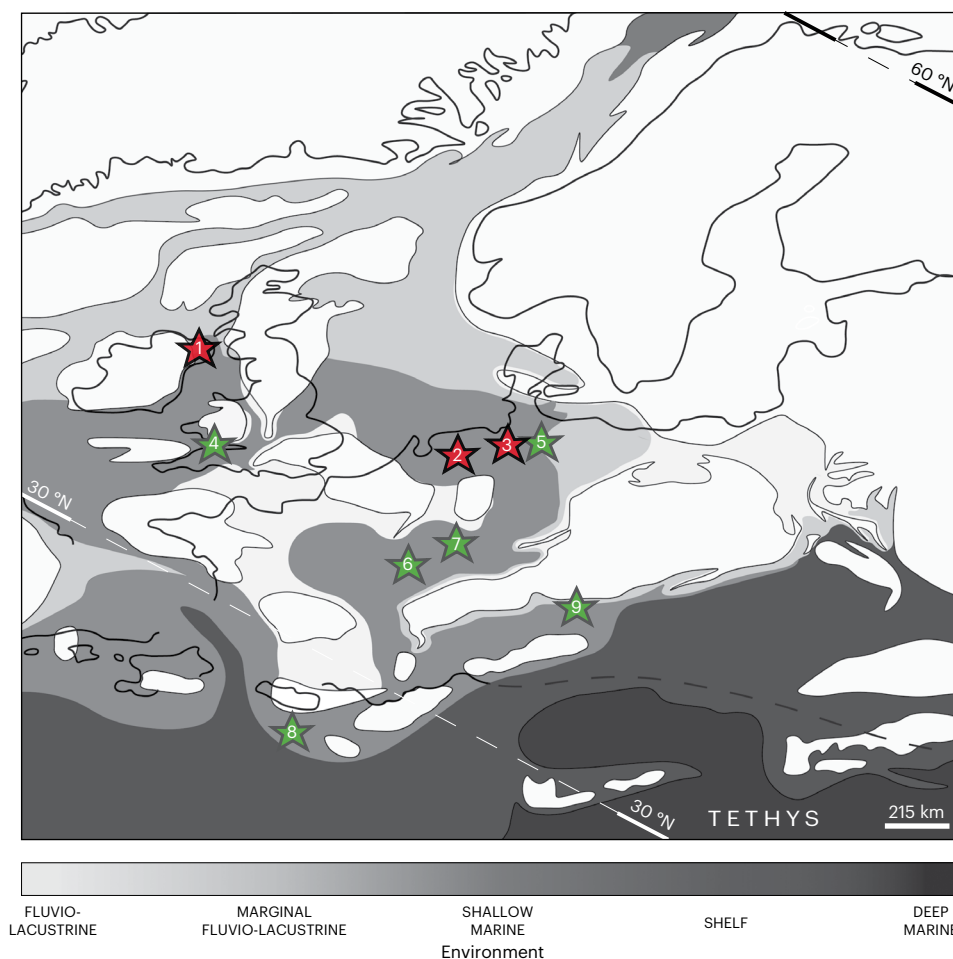
Fig. 1 | Triassic–Jurassic palaeogeography of the Tethyan shelf. 1, Carnduff-2 core, Larne Basin, N. Ireland; 2, Hebelermeer-2 core, Germanic Basin, Germany; 3, Schandelah-1 core, Lower Saxony Basin, Germany; 4, St Audrie's Bay, Bristol Channel Basin, England; 5, Mariental-1 core, Germanic Basin, Germany; 6, Rosswinkel FR 201–204 core, Luxembourg; 7, Mingolsheim core, Germanic Basin, Germany; 8, Val Adrara section, Lombardy Basin, Italy; 9, Kuhjoch section, Eiberg Basin, Austria (GSSP (Global Boundary Stratotype Section and Point)). Red stars represent sites from this study. Green stars represent sites of previous palaeo-redox studies and/or of stratigraphic importance. Figure adapted with permission from: colour scale, ref. [12], Wiley; palaeogeographic reconstruction, ref. [23], Elsevier.

The unconstrained areal extent of globally sulfidic conditions during the ETME limits understanding of the spatial complexity of redox change as a driver of Late Triassic marine extinctions.

The isotopic composition of molybdenum (Mo) in organic-rich sediments has been widely used to reconstruct the oxygenation of both local and global ancient marine environments[15,16]. Under oxic depositional conditions, Mo typically exhibits low sedimentary enrichments and isotopically light compositions, due principally to (Mn)oxyhydroxide adsorption, with compositions ~3‰ lighter than coeval seawater[16–18]. Under reducing conditions, Mo exhibits higher sedimentary enrichments due to the formation of thiolated (poly)molybdate species that have smaller isotopic offsets from seawater than Mo adsorbed onto oxyhydroxides[19,20]. Generally well-oxygenated global marine conditions are therefore reflected by isotopically heavy $\delta^{98}Mo$ seawater values due to oxyhydroxide adsorption acting as the primary vector of Mo burial[21]. However, isotopically light Mo burial can also occur due to intermediate thiomolybdate formation[22]. High sulfidic global marine conditions, by contrast, are represented by isotopically light $\delta^{98}Mo$ seawater values as global oxyhydroxide burial declines[21], but no observations of $\delta^{98}Mo$ evolution exist from across the TJB and ETME.

In this Article, we use the sedimentary enrichment (Mo_{EF}) and isotopic composition of Mo to examine the link between marine de-oxygenation and extinction during the ETME. We obtained material from the Carnduff-2 core (Northern Ireland), Hebelermeer-2 core (west Germany) and Schandelah-1 core (north Germany), which preserve lithological records of marine marls, sandstones and organic-rich shales deposited on the Tethyan shelf before, during and after the ETME (Fig. 1). All three sites have undergone previous stratigraphic study and include detailed biotic records for correlation[6,23–25]. The samples analysed in this study are therefore ideally suited to explore the relationship between marine extinction and de-oxygenation on the Tethyan shelf across the TJB. We identify little correlation between proxies for detrital sediment input and $\delta^{98}Mo$ or Mo_{EF} and therefore interpret stratigraphic variations in Mo concentrations mainly as a function of local redox conditions (Supplementary Fig. 4).

Limited euxinia during Triassic–Jurassic transition

The $\delta^{98}Mo$ of coeval seawater ($\delta^{98}Mo_{SW}$) must be resolved to determine global redox conditions. However, to determine $\delta^{98}Mo_{SW}$, sedimentary $\delta^{98}Mo$ values must be corrected for isotopic fractionation, with the isotopic fractionation and sedimentary enrichment of Mo being dependent on local redox conditions[21]. The maximum $\delta^{98}Mo$ compositions of Upper Triassic mudstones in the studied cores are ~1.6‰ (Carnduff-2: 1.56‰; Hebelermeer-2: 1.63‰; Fig. 2). These $\delta^{98}Mo$ values are obtained from sampling levels where trace-metal distributions are indicative of
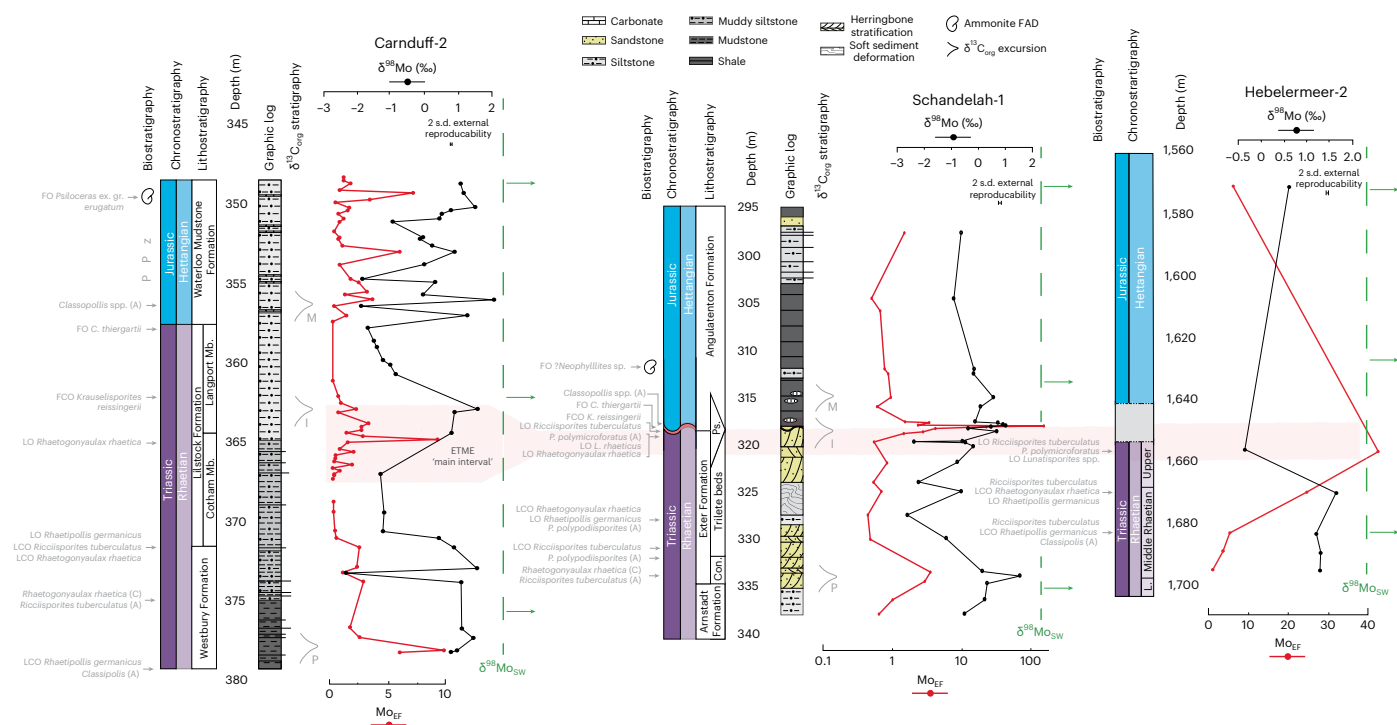
Fig. 2 | Overview of key stratigraphic, lithological and geochemical data for Carnduff-2, Schandelah-1 and Hebelermeer-2. Carnduff-2 stratigraphic and lithological data from refs. 13,25; Mo$_{EF}$ data from ref. 13; Schandelah-1 stratigraphic and lithological data from refs. 23,24; Hebelermeer-2 stratigraphic data from ref. 6. (A), abundant; (C), common; Con, Contorta Beds; FCO, first common occurrence; FO, first occurrence; LCO, last common occurrence; LO, last occurrence; Mb., Member; Ps., Psilonoten sandstone; M, main; I, initial; P, precursor (pertaining to carbon isotope excursions). Green dashed line represents minimum δ^{98}Mo$_{SW}$. Mo$_{EF}$ calculations detailed in Methods.

suboxic depositional conditions (Supplementary Figs. 1–3)[13]. Suboxic conditions coinciding with upper-bound Carnduff-2 δ^{98}Mo values are further supported by oxic–ferruginous iron speciation values from a correlative horizon within the Larne Basin[14]. Molybdenum sulfides forming in sedimentary porewaters underlying a non-euxinic water column are fractionated by a minimum of ~0.7‰ relative to coeval seawater[26,27], with fractionation probably exceeding 0.7‰ within the Larne Basin because of local redox conditions[13,14]. Burial of Mo under ferruginous conditions would lead to sediment compositions with similar isotopic offsets from δ^{98}Mo$_{SW}$ and so would not alter this conclusion[28]. Therefore, Late Triassic δ^{98}Mo$_{SW}$ was probably >2.3‰, similar to or greater than modern-day seawater[29]. A Late Triassic δ^{98}Mo$_{SW}$ equal to or greater than the modern ocean is consistent with sulfidic conditions covering no more than ~0.05–0.10% of the Late Triassic seafloor, similar to or even less than in the modern day[16,29].

The average upper-bound δ^{98}Mo throughout the basal Jurassic of the Carnduff-2 core is 1.47 ± 0.58‰ (n = 3) and characterizes horizons with trace-metal distributions that are indicative of localized suboxia[13]. Predominantly non-euxinic conditions from the basal Jurassic of the Larne Basin are further supported by iron speciation data[14]. Therefore, basal Jurassic δ^{98}Mo$_{SW}$ was probably >2.2‰, also similar to the Late Triassic and modern global ocean. The persistence of a similar δ^{98}Mo$_{SW}$ from the Late Triassic to the basal Jurassic suggests that, unlike uranium isotope records[10,11], there was no substantial change in the global Mo cycle across the TJB and that sulfidic anoxia in the Early Jurassic global open ocean remained spatially limited. Our conclusion is further supported by pyrite framboid data from an open ocean Panthalassa site[30].

Regional de-oxygenation during the ETME

Oxygen-poor conditions were present across Tethyan and Panthalassa marginal marine environments during the main extinction interval[5,7,13,14]. Such conditions have been further identified here on the basis of

δ^{98}Mo and Mo$_{EF}$ data with redox conditions varying according to both site and stratigraphy. The Schandelah-1 and Carnduff-2 cores both exhibit positive δ^{98}Mo shifts that directly coincide with the main extinction interval, as denoted by the 'initial' negative carbon isotope excursion (CIE)[2,31,32] (Fig. 2). The increase in δ^{98}Mo (and Mo$_{EF}$) during the main extinction interval indicates an increased availability of reduced sulfur [HS$^-$], probably due to the shoaling of the sulfate reduction zone within sedimentary porewaters up to the sediment–water interface[26,27,33]. Relatively high Mo$_{EF}$ alongside low δ^{98}Mo values around the base of the main extinction interval within the Hebelermeer-2 core also indicates increased [HS$^-$] prevalence, probably due to the expansion of the sulfate reduction zone into the water column, with the burial of intermediate thiomolybdate species at H$_2$S concentrations <11 μM (refs. 20,22) (Supplementary Information section 1.4). Isotopically light values are inconsistent with oxide adsorption given the elevated total sulfur (%) at this horizon[6]. Sulfidic conditions around the base of the initial CIE at St Audrie's Bay (Somerset, UK) have been interpreted through a positive δ^{34}S excursion[4].

Low sulfate within Late Triassic seawater of the Tethyan shelf has been interpreted through δ^{34}S data[7]. Low marine sulfate concentrations[7] are unlikely to have affected broad trends in δ^{98}Mo observed here given the inter-site consistency in data and the argument that calculated sulfate concentrations in Late Triassic oceans (0.2–1.1 mM) were still in excess of those required for thiomolybdate formation up to and exceeding ~11 μM (refs. 7,16) (Supplementary Information section 1.5).

Pulsed marginal marine euxinia during ETME

Multiple pulses of marine sulfidic anoxia were prevalent on the Tethyan shelf during the latest Triassic and earliest Jurassic. Low to moderate Mo$_{EF}$ as well as isotopically heavy δ^{98}Mo in all three cores during deposition of the basal Westbury Formation and stratigraphically equivalent units are suggestive of shoaling of the sulfate reduction zone towards
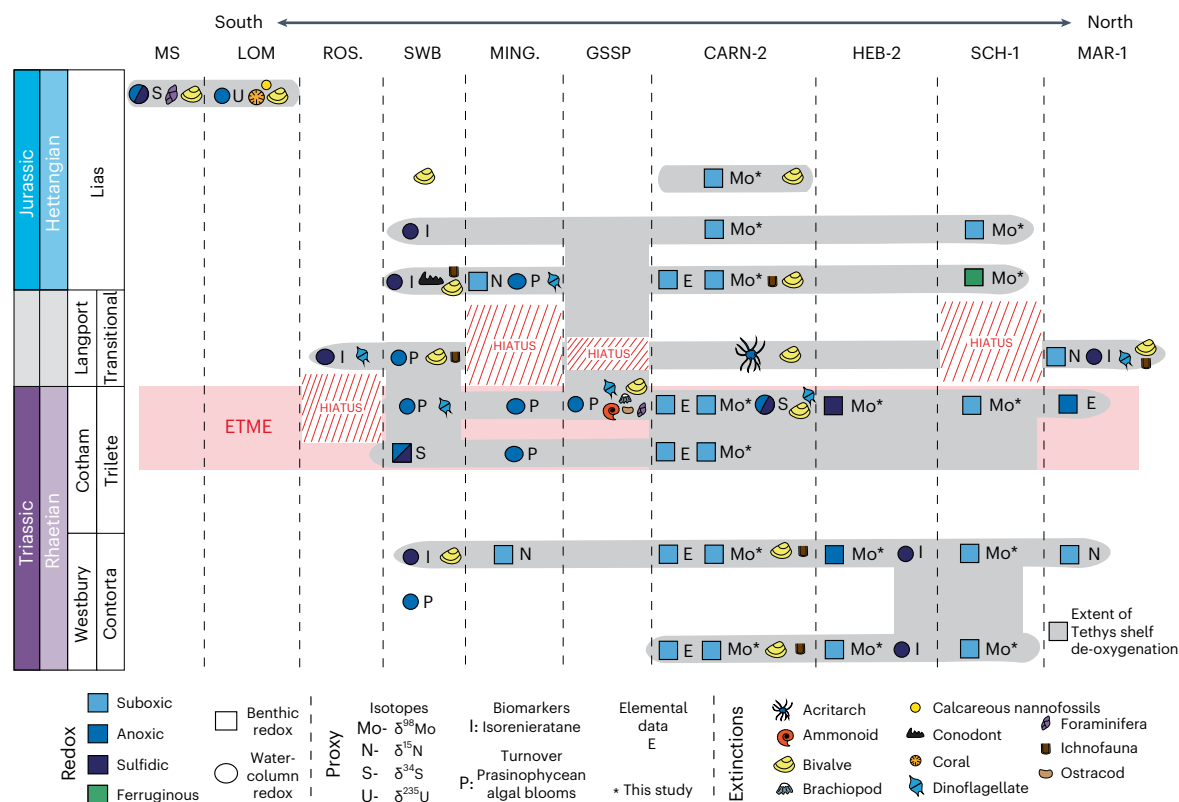
Fig. 3 | Stepped evolution of marine de-oxygenation and extinction on the Tethyan shelf through the Late Triassic. CARN-2, Carnduff-2 core, Larne Basin, N. Ireland; GSSP, Kuhjoch Section, Eiberg Basin, Austria; HEB-2, Hebelermeer-2 core, Germanic Basin, Germany; LOM., Val Adrara section, Lombardy Basin, Italy; MAR-1, Mariental-1 core, Germanic Basin, Germany; MING., Mingolsheim core, Germanic Basin, Germany; MS, Mount Sparagio section, Lombardy Basin, Italy; ROS., Rosswinkel FR 201–204 core, Luxembourg; SCH-1, Schandelah-1 core,

Lower Saxony Basin, Germany; SWB, St Audrie's Bay and Lavernock Point, Bristol Channel Basin, southwest Britain. $\delta^{15}N$ data from refs. 3,34; $\delta^{34}S$ data from refs. 4,7; $\delta^{235}U$ data from ref. 10; isorenieratane data from refs. 3,4,6,8; prasinophycean data from refs. 3,9; elemental data from refs. 3,13; extinction data from refs. 3,8,9,13,32,45,46. Stratigraphic correlation based on Supplementary Figs. 9–11 and ref. 47.

the sediment–water interface[26,27,33]. Similar shoaling of the sulfate reduction zone is also inferred from the Carnduff-2 and Hebelermeer-2 cores during the deposition of the uppermost Westbury Formation and equivalent units. Both phases of porewater de-oxygenation coincided with photic-zone euxinia on the Tethyan shelf during the middle Rhaetian[6] (Fig. 3); the upper pulse also coincided with episodic photic-zone euxinia within the Bristol Channel Basin[8] and de-nitrification within the Central European Basin at the Mingolsheim and Mariental-1 sites[3,34] (Fig. 3). $\delta^{98}Mo$ then decreases during the deposition of the lower Cotham Member and stratigraphically equivalent units, as seen within both the Carnduff-2 and Schandelah-1 cores, with Mo_{EF} decreasing or remaining low. Despite previous studies interpreting broadly oxygenated depositional conditions during the basal Cotham Member, isotopically light $\delta^{98}Mo$ within the Larne Basin may be associated with intermediate thiomolybdates and organic matter preservation, suggesting weakly oxygen-poor conditions[22,35].

Multiple further positive shifts in $\delta^{98}Mo$ and Mo_{EF} are observed within the basal Jurassic of the Carnduff-2 core, suggestive of pulsed increases of [HS$^-$] caused through periodic shoaling of the sulfate reduction zone. Correlative horizons within the Schandelah-1 core contain $\delta^{98}Mo$ and Mo_{EF} shifts also indicative of variable shoaling of the sulfate reduction zone. Pulsed oxygen-poor conditions within the basal Jurassic of the Carnduff-2 and Schandelah-1 cores coincided with photic-zone euxinia within the Bristol Channel Basin[4,8] (Fig. 3).

Periodically pulsed anoxia during the Late Triassic and Early Jurassic has previously been noted on the basis of eccentricity modulated precession timescales in the Bristol Channel Basin (St Audrie's Bay),

with laminated organic-rich black shales forming every precession cycle[36]. Pulses of marine redox change have also been reported from the Larne Basin, coinciding largely with the disappearance of infaunal bivalve taxa[13]. We similarly note a close relationship between redox pulses and Late Triassic extinction phases (Fig. 3).

Localized marine euxinia as driver of extinction during ETME

The coincidental pulsed nature of sulfidic marine de-oxygenation and end-Triassic marine extinction phases strongly suggests a causal relationship (Figs. 3 and 4). However, the limited extent of marine sulfidic anoxia through the TJB inferred from our new Mo isotope datasets suggests that these pulses of marine de-oxygenation were limited largely to marginal marine environments. More persistent and widespread oxygen-poor conditions towards the end of the ETME have been suggested from carbonate $\delta^{238}U$ data that have been modelled to suggest uranium reduction across ~8–20% of the global seafloor[10,11]. However, such anoxic conditions probably manifested within marginal marine and intermediate-depth Tethyan and Panthalassa environments[3–5,7], with little evidence for open marine de-oxygenation[30], and provide limited information on the extent of sulfidic conditions. Our new Mo isotope data add to these observations by showing that even if moderate de-oxygenation (enough to perturb the uranium cycle) took place near the ETME, there was little increase in the volume of waters containing dissolved sulfide. We suggest that geographically localized sulfidic marine de-oxygenation within Late Triassic marginal marine environments
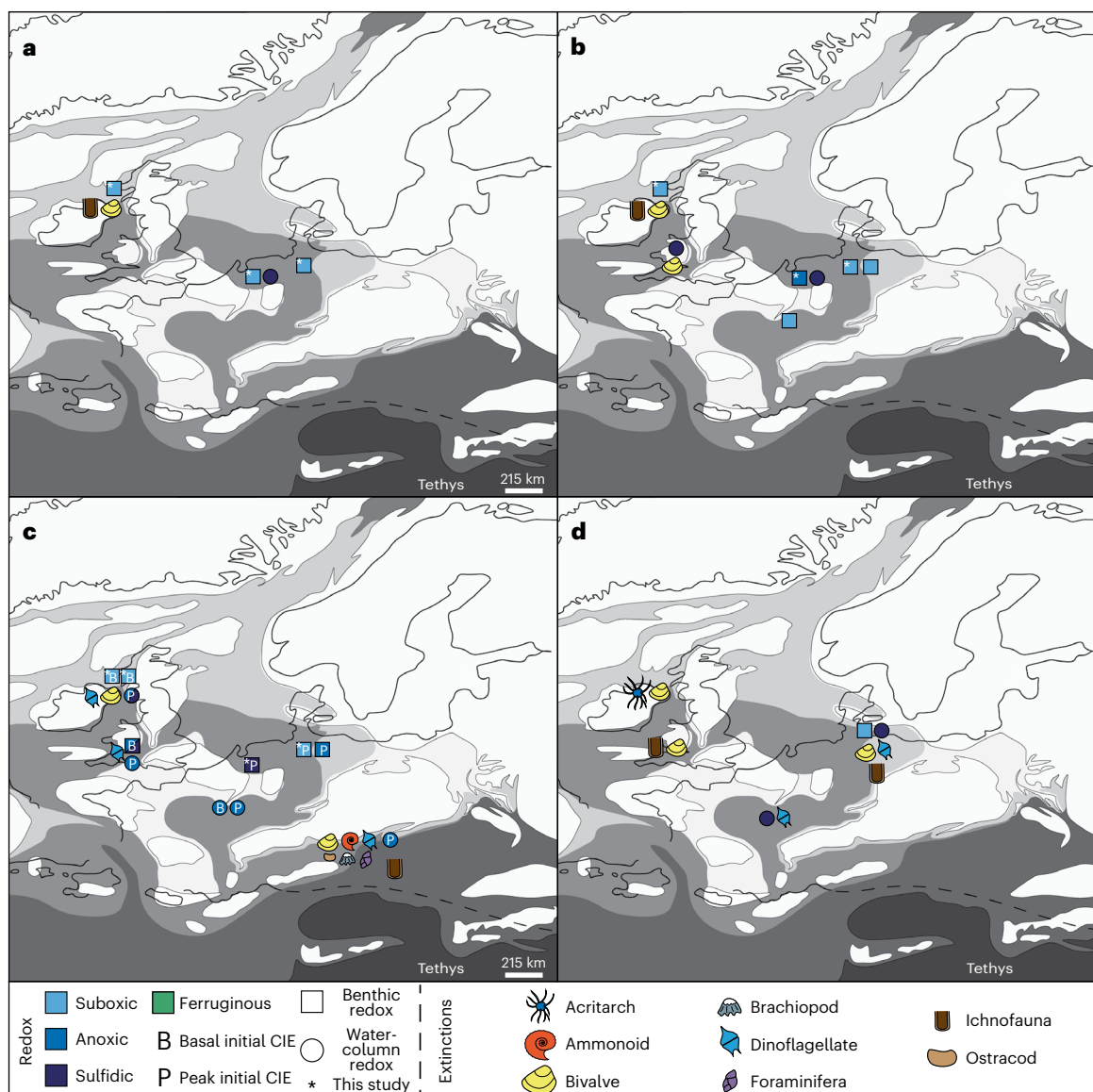
Fig. 4 | Pulses of marine de-oxygenation and synchronous extinction during the latest Triassic and earliest Jurassic on the Tethyan shelf. a,b, Pre-initial CIE during the basal (**a**) and upper (**b**) Westbury Formation/Contorta beds. **c**, Initial CIE. **d**, Post-initial CIE. For data source(s), refer to Fig. 3. Palaeo-latitude as in Fig. 1. Figure adapted with permission from: palaeogeography, ref. 12, Wiley and ref. 23, Elsevier; extinction pictograms, ref. 32, Elsevier .

therefore had major implications for Late Triassic biodiversity and ecosystem stability.

Our inference of geographically localized marine de-oxygenation is consistent with recent studies indicating elevated weathering and erosion rates in Tethyan shelf localities during the Late Triassic[37,38]. Localized marine de-oxygenation may have been driven by high run-off from the Late Triassic continents triggering eutrophication and stratification, with increased run-off driven by a warming climate, enhanced hydrological cycle and the collapse of forest ecosystems leading to enhanced soil erosion[39]. Marine de-oxygenation within Tethyan and Panthalassa marginal marine environments may also have been associated with the expansion of oxygen minimum zones[5,7]. Open marine environments would have been substantially less affected by weathering perturbations, with oxygen minimum zone expansion potentially being focused around intermediate-depth, marginal marine environments, and consequently the open oceans may have remained refugia for marine life.

Modern marginal marine environments are probably also particularly sensitive to changes in marine redox while also being some of the most biodiverse oceanic environments on Earth[40–43]. Therefore, anthropogenically driven environmental change, including the local expansion of marine anoxia and enhanced marine nutrient supply, may result in geographically localized marine de-oxygenation, which could have major consequences for future marine biodiversity and ecosystem stability[44], with particularly severe consequences for marginal marine corals, mangroves and coastal fishes[1,42,43].

Online content

Any methods, additional references, Nature Portfolio reporting summaries, source data, extended data, supplementary information, acknowledgements, peer review information; details of author contributions and competing interests; and statements of data and code availability are available at https://doi.org/10.1038/s41561-023-01303-2.

References

1. Dunhill, A. M., Foster, W. J., Sciberras, J. & Twitchett, R. J. Impact of the Late Triassic mass extinction on functional diversity and composition of marine ecosystems. *Palaeontology* **61**, 133–148 (2018).

2. Ruhl, M., Bonis, N. R., Reichart, G.-J., Sinninghe Damsté, J. S. & Kürschner, W. M. Atmospheric carbon injection linked to end-Triassic mass extinction. *Sci. Rep.* **333**, 430–434 (2011).

3. Richoz, S. et al. Hydrogen sulphide poisoning of shallow seas following the end-Triassic extinction. *Nat. Geosci.* **5**, 662–667 (2012).

4. Jaraula, C. M. B. et al. Elevated p_{CO_2} leading to Late Triassic extinction, persistent photic zone euxinia, and rising sea levels. *Geology* **41**, 955–958 (2013).

5. Kasprak, A. H. et al. Episodic photic zone euxinia in the northeastern Panthalassic Ocean during the end-Triassic extinction. *Geology* **43**, 307–310 (2015).

6. Blumenberg, M., Heunisch, C., Lückge, A., Scheeder & Wiese, F. Photic zone euxinia in the central Rhaetian Sea prior the Triassic–Jurassic boundary. *Palaeogeogr. Palaeoclimatol. Palaeoecol.* **461**, 55–64 (2016).

7. He, T. et al. An enormous sulfur isotope excursion indicates marine anoxia during the end-Triassic mass extinction. *Sci. Adv.* **6**, eabb6704 (2020).

8. Fox, C. P. et al. Two-pronged kill mechanism at the end-Triassic mass extinction. *Geology* https://doi.org/10.1130/G49560.1 (2022)

9. Bonis, N. R., Ruhl, M. & Kürschner, W. M. Climate change driven black shale deposition during the end-Triassic in the western Tethys. *Palaeogeogr. Palaeoclimatol. Palaeoecol.* **290**, 151–159 (2010).

10. Jost, A. B. et al. Uranium isotope evidence for an expansion of marine anoxia during the end-Triassic extinction. *Geochem. Geophys. Geosyst.* **18**, 3093–3108 (2017).

11. Somlyay, A. et al. Uranium isotope evidence for extensive seafloor anoxia after the end-Triassic mass extinction. *Earth Planet. Sci. Lett.* **614**, 118190 (2023).

12. van de Schootbrugge, B., Bachan, A., Suan, G., Richoz, S. & Payne, J. L. Microbes, mud and methane: cause and consequence of recurrent Early Jurassic anoxia following the end-Triassic mass extinction. *Palaeontology* **56**, 685–709 (2013).

13. Bond, A. D., Dickson, A. J., Ruhl, M. & Raine, R. Marine redox change and extinction in Triassic–Jurassic boundary strata from the Larne Basin, Northern Ireland. *Palaeogeogr. Palaeoclimatol. Palaeoecol.* **598**, 111018 (2022).

14. He, T. et al. Extensive marine anoxia in the European epicontinental sea during the end-Triassic mass extinction. *Glob. Planet. Change* **210**, 103771 (2022).

15. Dickson, A. J. A molybdenum-isotope perspective on Phanerozoic deoxygenation events. *Nat. Geosci.* **10**, 721–726 (2017).

16. Kendall, B., Dahl, T. W. & Anbar, A. D. The stable isotope geochemistry of molybdenum. *Rev. Mineral. Geochem.* **82**, 683–732 (2017).

17. Barling, J. & Anbar, A. D. Molybdenum isotope fractionation during adsorption by manganese oxides. *Earth Planet. Sci. Lett.* **217**, 315–329 (2004).

18. Scott, C. & Lyons, T. W. Contrasting molybdenum cycling and isotopic properties in euxinic versus non-euxinic sediments and sedimentary rocks: refining the paleoproxies. *Chem. Geol.* **324**–**325**, 19–27 (2012).

19. Erickson, B. E. & Helz, G. R. Molybdenum(VI) speciation in sulfidic waters: stability and lability of thiomolybdates. *Geochim. Cosmochim. Acta* **64**, 1149–1158 (2000).

20. Nägler, T. F., Neubert, N., Böttcher, M. E., Dellwig, O. & Schnetger, B. Molybdenum isotope fractionation in pelagic euxinia: evidence from the modern Black and Baltic seas. *Chem. Geol.* **289**, 1–11 (2011).

21. Dickson, A. J. et al. Isotopic constraints on ocean redox at the end of the Eocene. *Earth Planet. Sci. Lett.* **562**, 116814 (2021).

22. Kerl, C. F., Lohmayer, R., Bura-Nakić, E., Vance, D. & Planer-Friedrich, B. Experimental confirmation of isotope fractionation in thiomolybdates using ion chromatographic separation and detection by multicollector ICPMS. *Anal. Chem.* **89**, 3123–3129 (2017).

23. Lindström, S. et al. A new correlation of Triassic–Jurassic boundary successions in NW Europe, Nevada and Peru, and the Central Atlantic Magmatic Province: a time-line for the end-Triassic mass extinction. *Palaeogeogr. Palaeoclimatol. Palaeoecol.* **478**, 80–102 (2017).

24. van de Schootbrugge, B. et al. The Schandelah Scientific Drilling Project: a 25-million year record of Early Jurassic palaeo-environmental change from northern Germany. *Newsl. Stratigr.* **52**, 249–296 (2019).

25. Boomer, I. et al. Stratigraphy, palaeoenvironments and geochemistry across the Triassic–Jurassic boundary transition at Carnduff, County Antrim, Northern Ireland. *Proc. Geol. Assoc.* **132**, 667–687 (2021).

26. Poulson Brucker, R. L., McManus, J., Severmann, S. & Berelson, W. M. Molybdenum behaviour during early diagenesis: insights from Mo isotopes. *Geochem. Geophys. Geosyst.* **10**, Q06010 (2009).

27. Scholz, F., Siebert, C., Dale, A. W. & Frank, M. Intense molybdenum accumulation in sediments underneath a nitrogenous water column and implications for the reconstruction of paleo-redox conditions based on molybdenum isotopes. *Geochim. Cosmochim. Acta* **213**, 400–417 (2017).

28. Goldberg, T., Archer, C., Vance, D. & Poulton, S. W. Mo isotope fractionation during adsorption to Fe (oxyhydr)oxides. *Geochim. Cosmochim. Acta* **73**, 6502–6516 (2009).

29. Nakagawa, Y. et al. The molybdenum isotope composition of the modern ocean. *Geochem. J.* **46**, 131–141 (2012).

30. Wignall, P. B. et al. An 80 million year oceanic redox history from Permian to Jurassic pelagic sediments of the Mino-Tamba terrane, SW Japan, and the origin of four mass extinctions. *Glob. Planet. Change* **71**, 109–123 (2010).

31. Hesselbo, S. P., Robinson, S. A., Surlyk, F. & Piasecki, S. Terrestrial and marine extinction at the Triassic–Jurassic boundary synchronized with major carbon-cycle perturbation: a link to initiation of massive volcanism? *Geology* **30**, 251–254 (2002).

32. Wignall, P. B. & Atkinson, J. W. A two-phase end-Triassic mass extinction. *Earth Sci. Rev.* **208**, 103282 (2020).

33. Siebert, C., McManus, J., Bice, A., Poulson, R. & Berelson, W. M. Molybdenum isotope signatures in continental margin marine sediments. *Earth Planet. Sci. Lett.* **241**, 723–733 (2006).

34. Quan, T. M., van de Schootbrugge, B., Field, M. P. & Rosenthal, Y. Nitrogen isotope and trace metal analyses from the Mingolsheim core (Germany): evidence for redox variations across the Triassic–Jurassic boundary. *Glob. Biogeochem. Cycles* https://doi.org/10.1029/2007GB002981 (2008).

35. King, E. K., Perakis, S. S. & Pett-Ridge, J. C. Molybdenum isotope fractionation during adsorption to organic matter. *Geochim. Cosmochim. Acta* **222**, 584–598 (2018).

36. Ruhl, M. et al. Astronomical constraints on the duration of the early Jurassic Hettangian stage and recovery rates following the end-Triassic mass extinction (St Audrie's Bay/East Quantoxhead, UK). *Earth Planet. Sci. Lett.* **295**, 262–276 (2010).

37. van de Schootbrugge, B. et al. Catastrophic soil loss associated with end-Triassic deforestation. *Earth Sci. Rev.* **210**, 103332 (2020).

38. Fox, C. P., Whiteside, J. H., Olsen, P. E. & Grice, K. Flame out! End-Triassic mass extinction polycyclic aromatic hydrocarbons reflect more than just fire. *Earth Planet. Sci. Lett.* **584**, 117418 (2022).

39. van de Schootbrugge, B. et al. Floral changes across the Triassic/Jurassic boundary linked to flood basalt volcanism. *Nat. Geosci.* **2**, 589–594 (2009).

40. Schmidtko, S., Stramma, L. & Visbeck, M. Decline in global oceanic oxygen content during the past five decades. *Nature* **542**, 335–337 (2017).

41. Breitburg, D. L. et al. Declining oxygen in the global ocean and coastal waters. *Science* **359**, eaam7240 (2018).

42. Renema, W. et al. Hopping hotspots: global shifts in marine biodiversity. *Science* **321**, 654–657 (2008).

43. Tittensor, D. P. et al. Global patterns and predictors of marine biodiversity across taxa. *Nature* **466**, 1098–1101 (2010).

44. IPCC *Climate Change 2021: The Physical Science Basis* (eds Masson-Delmotte, V. et al.) (Cambridge Univ. Press, 2021).

45. Barras, C. G. & Twitchett, R. J. Response of the marine infauna to Triassic–Jurassic environmental change: ichnological data from southern England. *Palaeogeogr. Palaeoclimatol. Palaeoecol.* **244**, 223–241 (2007).

46. Hillebrandt, A. V. et al. The Global Stratotype Sections and Point (GSSP) for the base of the Jurassic System at Kuhjoch (Karwendel Mountains, Northern Calcareous Alps, Tyrol, Austria). *Episodes* **36**, 162–198 (2013).

47. Bond, A. D. *Quantifying Marine Redox Across the Triassic Jurassic Mass Extinction*. PhD thesis, Royal Holloway, Univ. London (2023).

Methods

Bulk inorganic geochemistry

From each sample, 50 mg was digested using inverse aqua regia (3/1 HNO_3/HCl) followed by digestion of silicates in 1/2 HF/HNO_3. Major elemental concentration data were measured using Perkin Elmer Optima 3300RL inductively coupled plasma atomic emission spectroscopy, and minor elemental concentration data were measured using Perkin Elmer NexION 350D inductively coupled plasma mass spectrometry. Accuracy was determined using full procedural digests of MAG-1 ($n = 7$) and was ±2.5% with Mo within uncertainty of the certified value. Precision was calculated using the 2 s.d. of the MAG-1 digests as ±17% (Cr, Cu, Zn, Al ±<10%), as well as five digests of an in-house mudrock standard (PERN-1) as ±21%. The Mo_{EF} was determined using $((Mo_{sample}/Al_{sample})/(Mo_{ucc}/Al_{ucc}))$. Upper continental crust concentrations were taken from ref. 48.

Molybdenum concentrations and isotopes

Samples were processed and measured under trace-metal-clean laboratory conditions. Before molybdenum-isotope analysis, each sample was weighed and mixed with a ^{97}Mo–^{100}Mo double-spike solution and digested in 3/1 HNO_3/HCl. The Mo samples were separated from matrix elements and interferences using an anion exchange column procedure detailed within refs. 49,50. The $\delta^{98/95}Mo$ compositions were measured using Thermo Scientific Neptune Plus multicollector inductively coupled plasma mass spectrometry. Procedural blanks for Mo were between 0.5 and 5.0 ng. All $\delta^{98/95}Mo$ data were calculated relative to NIST SRM 3,134 + 0.25‰ (ref. 51). Accuracy and precision were assessed using the Open University Mo solution standard (compare ref. 52) (-0.35 ± 0.15‰, $n = 12$, 2 s.d.) and multiple separate digests of USGS SDO-1 shale, which yielded an average $\delta^{98/95}Mo$ of 1.04 ± 0.08‰ (2 s.d., $n = 6$) within uncertainty of published values (1.05 ± 0.1‰) (ref. 52).

Data Availability

All data generated or analysed during this study are deposited in the Zenodo online repository and can be accessed via the following link: https://doi.org/10.5281/zenodo.8319867.

References

48. Rudnick, R. L. & Gao, S. in *The Crust: Treatise on Geochemistry* Vol. 3 (eds Holland, H. D. and Turekian, K. K.) 1–64. (Elsevier-Pergamon, 2003).

49. Pearce, C. R., Cohen, A. S. & Parkinson, I. J. Quantitative separation of molybdenum and rhenium from geological materials for isotopic determination by MC-ICP-MS. *Geostand. Geoanal. Res.* **33**, 219–229 (2009).

50. Dickson, A. J., Jenkyns, H. C., Porcelli, D., van den Boorn, S. & Idiz, E. Basin-scale controls on the molybdenum-isotope composition of seawater during the Oceanic Anoxic Event 2 (Late Cretaceous). *Geochim. Cosmochim. Acta* **178**, 291–306 (2016).

51. Nägler, T. F. et al. Proposal for an international molybdenum isotope measurement standard and data representation. *Geostand. Geoanal. Res.* **38**, 149–151 (2014).

52. Goldberg, T. et al. Resolution of inter-laboratory discrepancies in Mo isotope data: an intercalibration. *J. Anal. At. Spectrom.* **28**, 724–735 (2013).

Author contributions

A.J.D., A.D.B. and M.R. designed the research. M.R. sampled the Carnduff-2 core at the GSNI core repository. B.v.d.S. and R.B. provided access to material from the Schandelah-1 core. A.D.B. carried out elemental and isotopic geochemical analyses with assistance from A.J.D. A.D.B. and A.J.D. interpreted the data with assistance from M.R., R.B. and B.v.d.S. A.D.B. wrote the paper and designed the figures. All authors contributed to the text and figure amendments.

Competing interests

The authors declare no competing interests.

Additional information

Supplementary information The online version contains supplementary material available at https://doi.org/10.1038/s41561-023-01303-2.

Correspondence and requests for materials should be addressed to Andrew D. Bond or Alexander J. Dickson.

Peer review information *Nature Geoscience* thanks Brian Kendall, Ekaterina Larina and Robert Newton for their contribution to the peer review of this work. Primary Handling Editor: James Super, in collaboration with the *Nature Geoscience* team.

Reprints and permissions information is available at www.nature.com/reprints.